M. M. Hessien*, Nader El-Bagoury, M. H. H. Mahmoud and Osama M. Hemeda

Synthesis and Characterization of Nanocrystalline Barium–Samarium Titanate

DOI 10.1515/htmp-2015-0021
Received January 21, 2015; accepted April 25, 2015

Abstract: Barium–samarium titanate nanopowder ($Ba_{0.85}Sm_{0.1}TiO_3$) was synthesized through tartrate precursor route. The effect of annealing temperature on the formation, crystalline size, morphology and magnetic properties was systematically studied. The annealing temperature was varied from 600°C to 1,100°C. Thermal analysis measurement (TG-DSC, thermogravimetry-differential scanning calorimetry) was carried out on the precursor to characterize the thermal decomposition behavior. The results showed that the precursor of Ba–Sm–Ti mixture decomposed thermally in multistep weight loss up to about 480°C and perovskite $Ba_{0.85}Sm_{0.1}TiO_3$ started to form at ~520°C. X-ray diffraction and Fourier transform infrared (FTIR) spectroscopic measurements showed that the synthesized $Ba_{0.85}Sm_{0.1}TiO_3$ has a tetragonal dominant structure with the presence of intermediate $SmTi_2O_3$ at lower annealing temperature. The ratio of $SmTi_2O_3$ was decreased and completely disappeared at higher annealing temperatures. The tetragonality, the theoretical density and the crystalline size were increased by increasing annealing temperature. The crystalline size is still in nano-range of 12.4–19.9 nm even after annealing at 1,100°C. The morphology of the produced sample transferred from nano-cubes to nano-whisker to nano-mace (nano-aggregates) with the increase of annealing temperature.

Keywords: synthesis, tartrate route, barium titanate, samarium, morphology, XRD analysis

***Corresponding author: M. M. Hessien,** Materials and Corrosion Group, Department of Chemistry, Faculty of Science, Taif University, Al Huwaya, Taif, Saudi Arabia; Central Metallurgical Research and Development Institute (CMRDI), P.O. Box 87, Helwan, Cairo, Egypt, E-mail: hessienmahmoud@yahoo.com
Nader El-Bagoury, M. H. H. Mahmoud, Department of Chemistry, Faculty of Science, Taif University, Al Huwaya, Taif, Saudi Arabia; Central Metallurgical Research and Development Institute (CMRDI), P.O. Box 87, Helwan, Cairo, Egypt
Osama M. Hemeda, Physics Department, Faculty of Science, Tanta University, Tanta, Egypt

Introduction

Piezoelectric materials are keys to many modern technologies. Computers use piezoelectric memories, security systems use pyroelectric sensors, cell phones use better dielectrics to improve antenna reception, optical communication components require electro-optic films and piezoelectric transducers are used for many purposes, ranging from microspeakers to medical ultrasound [1–3]. Among which the perovskite group is the most important and thus most widely studied because of its superior electrical properties [4–7]. Perovskite is usually expressed as ABO_3. Lead zirconate titanate (PZT) family ceramics are widely used as piezoelectric materials, due to their high piezoelectric response. Lead is a very toxic element and is now being progressively removed from industrial processes [8] because of its toxicity and environmental risks.

Among the available lead-free ferroelectric ceramics, barium titanate $BaTiO_3$ (BT) [9–12] is the most widely studied lead-free material due to its potential applications as multilayer ceramic capacitors. The dielectric characteristics of barium titanate ceramics with respect to temperature, electric field strength, frequency and time (aging) are very dependent on the substitution of minor amounts of other ions, on microstructure, and in particular on fine grain size. When doped or substituted with some rare earth oxides, $BaTiO_3$ powder could achieve a high dielectric constant and breakdown electric field strength. The ferroelectric properties of BT can be efficiently controlled by doping or substituting with different elements [13–15]. It has been known that a high dielectric constant and good temperature stability can be achieved through addition of rare earth oxides.

The materials' performances are closely related to the ways they are processed. Synthesis method played a significant role in determining the microstructure, electrical and optical properties of ferroelectric ceramics [16–18]. Fully dense ferroelectric ceramics (> 95% of theoretical density) are required by most applications, because of several reasons. The dielectric constant of ferroelectric ceramics usually increases with increasing density and the presence of pores is generally a cause of high loss tangent. Ferroelectric powders were conventionally

synthesized via a solid-state reaction process, using constituent oxides as the starting materials [19–21]. Due to their relatively rough grains, these powders require relatively high sintering temperature to obtain ferroelectric ceramics with designed compositions and desired performances. The high sintering temperature worsens the electrical, optical or other useful characteristics. Thus, the preparation of piezoelectric materials powder with fine particle size, narrow particle size distribution and minimum particle agglomeration has received considerable attention in order to improve the material properties and to reduce the sintering temperature. It is necessary to use powders of ferroelectric compounds with small grain size and narrow size distribution. Wet-chemistry methods in the last decades, including chemical co-precipitation [22], organic acid precursor [23, 24], sol–gel process [25, 26], hydrothermal synthesis [27–29], microemulsion [30, 31], etc., have been shown that some ferroelectric materials can be synthesized directly from their oxide precursors in the form of nanosized powders, without the need for the higher or intermediate calcination temperatures. This study focused on developing and understanding the synthesis behavior of nanosized barium–samarium titanate powders via organic carboxylic acid precursor methods.

The advantages of organic acid process are that the low-cost starting materials, low synthesis temperature, fine microstructure, high performance, homogeneity, narrow particle size distribution and friendly environment procedure [32–34]. From our knowledge, no many data mentioned in literature about the synthesis of barium titanate nanopowders via organic acid precursors using titanium dioxide as a source of titanium.

The present study aims at synthesizing barium–samarium titanate ($Ba_{0.85}Sm_{0.1}TiO_3$) nanopowders via tartrate precursor methods. Thermal analysis of the unannealed precursors was carried out. The effects of annealing temperature (600–1,100°C) on the phase formation and microstructure will be investigated. The formed powders will be characterized by X-ray diffraction analysis (XRD), transmission electron microscope (TEM) and Fourier transform infrared (FTIR) spectroscopy.

Experimental

The tartrate precursor method was applied for the preparation of nanocrystalline titanate precursors for the synthesis of $Ba_{0.85}Sm_{0.1}TiO_3$. Pure chemical grade of barium chloride ($BaCl_2$), samarium nitrate ($Sm(NO_3)_3$) and titanium dioxide (TiO_2) in the presence of stoichiometric amount of tartaric acid ($C_4H_6O_6$) were used as starting materials. The mixtures of Ba–Sm–Ti solutions firstly prepared and then stirred for 15 min on hot plate magnetic stirrer, followed by addition of an aqueous solution of tartaric acid to the mixture with stirring. The solution was evaporated by heating at 80°C with constant stirring until dryness and then dried in a dryer at 100°C overnight. Thermal analysis of the formed compound (designated here as unannealed precursor) was carried out to characterize the thermal decomposition course up to the perovskite formation. The rate of heating was kept at 10° C/min between room temperature and 850°C. The measurements were carried out in a current of nitrogen atmosphere.

Phase composition and structure were determined using XRD analysis. The analyses were performed on a Brucker axis D8 diffractometer using Cu-K_α ($\lambda = 1.5406$) radiation and secondary monochromator in the range 2θ from 10° to 80°. Identification of the phases was determined by matching the experimental pattern with standards compiled by the Joint Committee on Powder Diffraction Standards (JCPDS). The shape and particle size were studied using TEM operated at 120 kV accelerating voltage (JTEM-1230, Japan, JEOL). The samples were prepared by making a suspension from the powder in distilled water using ultrasonic water bath. Then a drop of the suspension was put into the carbon grid and left to dry.

Results and discussion

Thermal analysis

Thermal decomposition studies of the precursors were analyzed using the TG-DSC technique in air atmosphere at 10°C/min. Figure 1 displays TG-DSC curve for $Ba_{0.85}$–$Sm_{0.1}$- titanate tartrate precursor. The absorbed water was removed by heating the tartrate precursor up to 165°C, which led to a weight loss of ~1.2 wt% in TG curve. After dehydration of the tartrate precursor, the tartrate metal complex decomposition involves mainly two steps. The first exothermic peak (2) occurred in the temperature range of 170–260°C along with an observed weight loss of ~33 wt% in TG curve, which was caused by the decomposition of the tartrate precursor into both metal oxides and gases (CO_2 and CO) through different steps. The third exothermic peak then occurred between 270°C and 460°C, resulting in a further weight loss of ~19.5 wt%, was most likely caused by the decomposition of

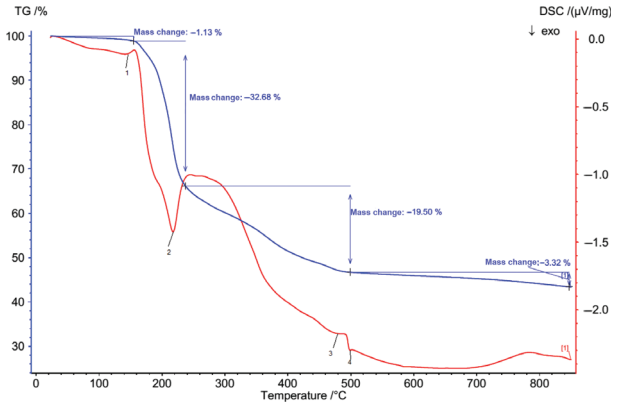

Figure 1: Thermo-gravimetric analysis (TG-DTG-DSC) for $Ba_{0.85}$-$Sm_{0.1}$-titanate tartrate precursor.

carboxylates. Thereafter (480°C), a further slight weight loss (~3%) was evident in the TG curve, indicating the completion of the tartrate-chain decomposition process. However, the DSC curve showed a minor exothermic peak at temperatures of 495°C. This peak corresponds to the solid–solid interaction of BaO, Sm_2O_3 and TiO_2 to form a nanosized perovskite $Ba_{0.85}Sm_{0.1}TiO_3$. In this case, nanosized $Ba_{0.85}Sm_{0.1}TiO_3$ can be obtained at much lower temperature as compared to conventional ceramic method.

XRD analysis

Figure 2 shows the XRD patterns of the perovskite structure $Ba_{0.85}Sm_{0.1}TiO_3$ at different annealing temperatures (600°C, 700°C, 800°C, 900°C, 1,000°C and 1,100°C) for 2 h. The figure shows strong broadening peaks which represent the $BaTiO_3$ phase. The presence of (002) peak in all composition suggests tetragonal symmetry at room temperature tetragonal symmetry showing splitted (001/100),(101/110),(002/200) and (112/211) peaks. Shifting of peak toward higher angle indicated the decrease in the lattice parameters with increasing the annealing temperature. It is obvious that the substitution of barium of the higher radius (1.6 Å) with samarium of the smaller radium (1.24 Å) resulted in decrease in cell parameters and hence cell size.

The tetragonality factor (c/a) for the prepared samples at different annealing temperature is shown in Figure 3. This factor increased by increasing annealing temperature which confirms the fact that the tetragonality increase and the other phases decrease by increasing annealing temperature. Similar results have already been reported for Samarium doped $BaTiO_3$ ceramics [35–37]. The XRD also indicated the presence of many phases beside tetragonal phase for the samples annealed at (600°C, 700°C and 800°C). On the other hand the samples annealed at 900°C, 1,000°C and 1,100°C have a pure tetragonal phase and the other phases disappeared. The intensity and the sharpness of the perovskite $BaTiO_3$ are highly increased by increasing annealing temperature. The broadening of the different peaks decreases by increasing annealing temperature without any change in the present phase.

The theoretical densities for $Ba_{0.85}Sm_{0.1}TiO_3$ at different annealing temperatures were calculated using the $D_{th} = M/NV$ where M is the molecular weight, N is Avogadro's number and V is the unit cell volume $= a^2c$ are given in Table 1. The theoretical density increased as

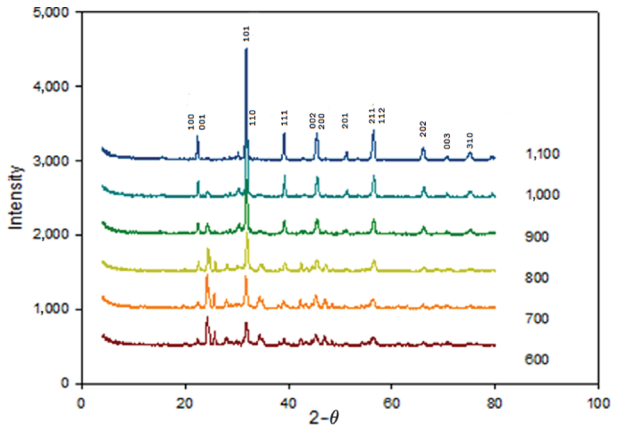

Figure 2: XRD patterns of $Ba_{0.85}Sm_{0.1}TiO_3$ from barium-smarium-titanium tartrate precursor thermally treated at different annealing temperatures for 2 h.

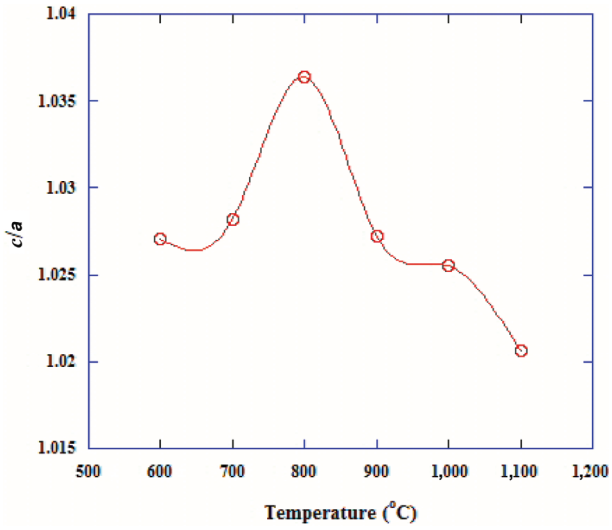

Figure 3: Tetragonality (c/a) for prepared sample at different annealing temperature.

Table 1: Physical parameters of prepared $Ba_{0.85}Sm_{0.1}TiO_3$ samples at different annealing temperatures.

Annealing temperature	Lattice parameter		Crystalline size	D_{th} (g/cm^3)[a]	Porosity	M = 248.4553
	a	*c*				
600	3.957103	4.064109	12.426	6.4852	0.625763	
700	3.96233	4.074138	15.31	6.452	0.623838	
800	3.931177	4.07426	16.32	6.555	0.629748	
900	3.946691	4.054274	16	6.535	0.628615	
1,000	3.94669	4.04735	19.87	6.547	0.629296	
1,100	3.96233	4.044175	18.8	6.5	0.626615	

Note: [a]Theoretical density.

the annealing temperature increased. The values of the crystallite size at different annealing temperature were calculated using Scherrer's equation:

$$B_{\text{crys.}} = \frac{0.9\lambda}{B\cos\theta}$$

where B is the full width at half maximum in radians. It is noticed that the crystalline size for the composition increased by increasing annealing temperature as shown in Figure 4. The crystalline size is still in nano-range after annealing at 1,100°C.

The XRD patterns indicate that the synthesized materials show good agreement with the conventional tetragonal $BaTiO_3$ structure (JCPDS data no. 05–0626) with no impurity peaks. The lattice parameters (a = 3.9945 Å and c = 4.0241 Å). The XRD pattern of the synthesized $BaTiO_3$ powder shows peak splitting at 45° correspond to the miller index (002 and 200) whereas a cubic $BaTiO_3$ has one single peak corresponding to (002). Therefore we can conclude that the synthesized $BaTiO_3$ powder by tartrate method shows a tetragonal dominant structure [38]. The peak at 2θ = 28.67° indicates the formation of intermediate phase ($SmTi_2O_3$) co-existing with the major phase which is an unstable intermediate [1, 39, 40]. This phase became in lower ratio and completely disappeared at higher annealing temperature.

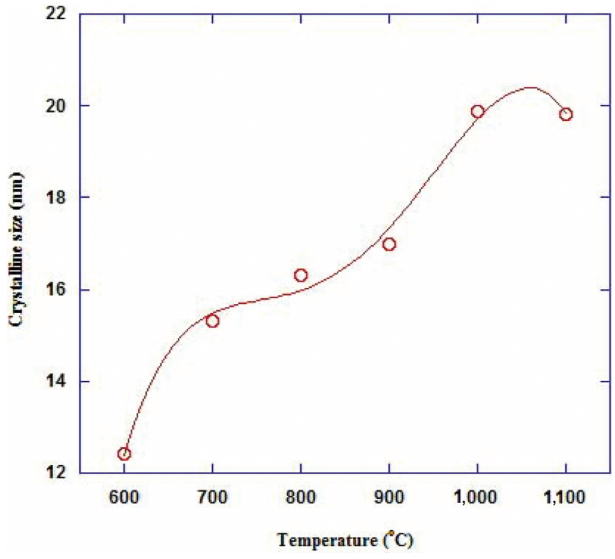

Figure 4: The crystalline size as a function of annealing temperature.

Fourier transform infrared (FTIR) spectroscopic analysis

FTIR spectroscopic measurements were used to investigate binding in the prepared Sm doped $BaTiO_3$ powders. FTIR spectra in the range of 200–5,000 cm^{-1} for the sample $Ba_{0.85}Sm_{0.1}TiO_3$ at different annealing temperature are shown in Figure 5(a)-b and Table 2. The absorption band at 3,418 cm^{-1} is assigned to the vibration of intermolecular hydrogen bond. The two peaks at υ_1 = 592 and υ_2 = 443 cm^{-1} are assigned to Ti–O octahedron. Beside the absorption strength of Ti–O octahedron another peaks appeared which attributed to M–O where M is the metal ions as Sm ion. The two broad peaks υ_1 and υ_2 are the characteristic peaks for the formation of the perovskite structure [37, 41, 42]. The intensity of these peaks increases by increasing annealing temperature. The several peaks appeared near υ_2 are collimated in one broad peak at 900°C and only the broad peaks υ_1 and υ_2 are appeared in the samples those annealed at 900°C, 1,000°C and 1,100°C indicating the formation of the single phase perovskite structure. These findings are in agreement with the above mentioned XRD results. The characteristic absorption peak at 1,426 cm^{-1} is assigned to symmetric stretching

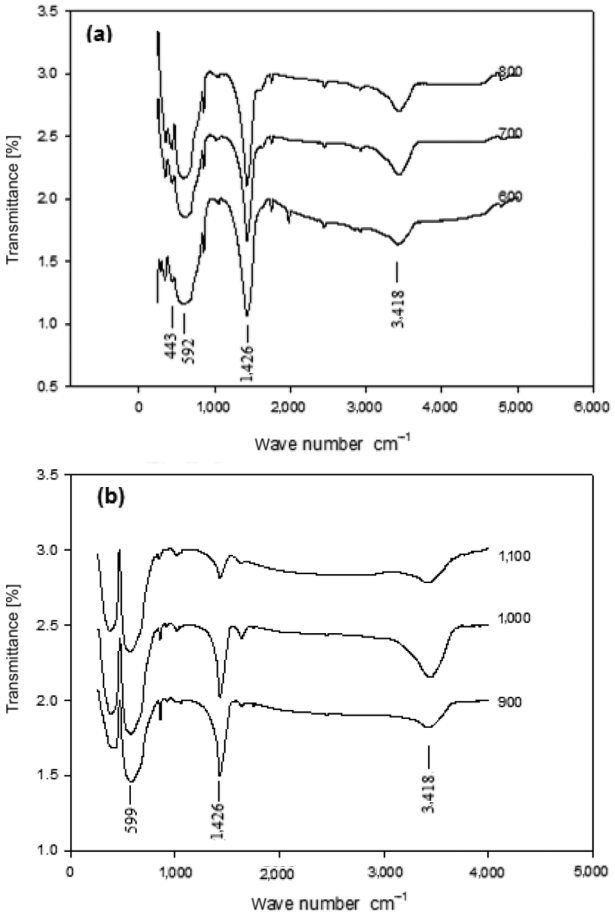

Figure 5: FTIR spectra for $Ba_{0.85}Sm_{0.1}TiO_3$ at different annealing temperature.

Table 2: FTIR data analysis.

	Annealing Temperature					
	600	**700**	**800**	**900**	**1,000**	**1,100**
u_1	443	441	438	414	–	–
u_2	592	599	593	575	573	573
u_3	859	858	857	858	847	858
u_4	1,426	1,429	1,427	1,425	1,431	1,426
u_5	1,751	1,751	1,752	1,750	–	1,750
u_6	1,980	1,983	–	–	–	–
u_7	2,449	2,450	2,450	2,448	–	2,449
u_8	2,854	–	–	2,817	2,834	–
u_9	2,923	2,924	2,924	–	–	2,926
u_{10}	3,418	3,420	3,420	3,422	3,422	3,445

vibration of C–O bond. The intensity of the peak decreases by increasing temperature and becomes small peak at 1,100°C due to the decomposition of any organic phases in the sample at high temperature.

Absorption peaks at the same mode of vibration for composition ($x = 0.1$) are obtained at 599, 593, 575, 573 and 573 for samples annealed at 700°C, 800°C, 900°C, 1,000°C and 1,100°C, respectively. A shift toward lower wave number and high energy is observed. This indicates that distance between Ti and O become shorter by annealing which enhancing the bond strength. It has been already reported that the variation of Ti–O is only related to the force constant [37]. In general the FTIR spectrum displays several types of vibration at 1,060, 1,751 and 3,000 cm^{-1} and they were assigned to Ti–O stretching Ti–OH and Ba–OH, respectively.

Morphological characterization

TEM images of $Ba_{0.85}Sm_{0.1}TiO_3$ at different annealing temperatures are shown in Figure 6(a)–(f). It can be seen that the annealing temperature has an important effect on the morphology of the produced barium-samarium titanate. It is found that the morphology of the produced sample transferred from nano-cubes to nano-whisker to nano-mace (nano-aggregates) as the annealing temperature increase. At 700°C (Figure 6(a)–(b)), the $Ba_{0.85}Sm_{0.1}TiO_3$ nano-cubes were obtained and discrete cubes could be observed. At 800°C, nano-whiskers $Ba_{0.85}Sm_{0.1}TiO_3$ were obtained (Figure 6(c)–(d)). Nano-maces (nano-aggregates) were observed by increasing the annealing temperature up to 1,000°C (Figure 6(e)–(f)). Based on the TEM morphological evolution, it can be concluded that $Ba_{0.85}Sm_{0.1}TiO_3$ nano-cubes initially observed in this work were directly transferred from the nanostructures tartarate precursor with the same morphology at relative low annealing temperature. Therefore they are single crystals. The nano-whiskers are formed at limited thermodynamics condition and finally will develop into nano-aggregates. Based on the TEM morphological structure, $Ba_{0.85}Sm_{0.1}TiO_3$ with controllable nanostructure can be obtained by controlling the annealing temperature.

Conclusion

Nanocrystalline $Ba_{0.85}Sm_{0.1}TiO_3$ has been synthesized via tartarate precursor route. The effect of annealing temperature on the formation, crystalline size and morphology was systematically studied. The results showed that:

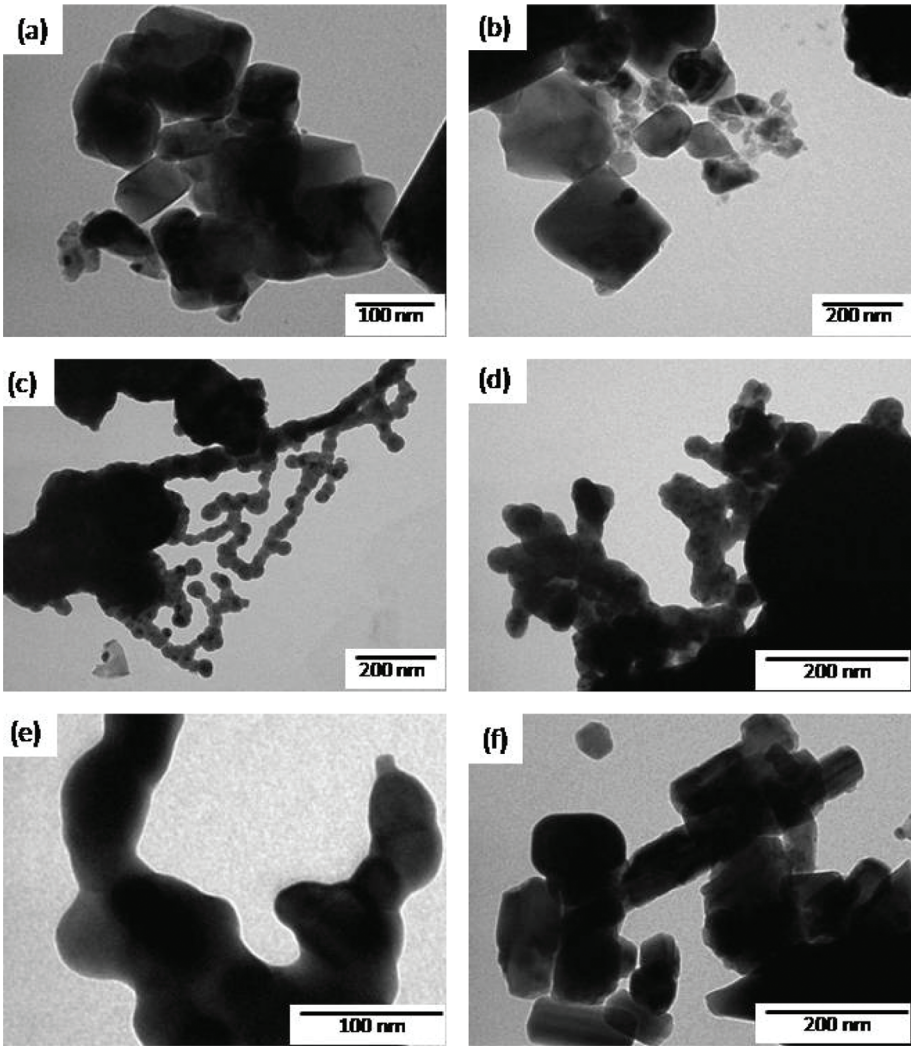

Figure 6: Different magnification TEM images of $Ba_{0.85}Sm_{0.1}TiO_3$ nanostructures as function of annealing temperature: (a–b) 700°C, (c–d) 800°C and (e–f) 1,000°C.

1. The tartarate precursor of Ba-Sm-Ti mixture decomposed thermally in multistep weight loss up to about 480°C and perovskite $Ba_{0.85}Sm_{0.1}TiO_3$ was started to form at ~520°C.
2. Perovskite $Ba_{0.85}Sm_{0.1}TiO_3$ was started to form at much lower annealing temperature (≥ 500°C).
3. The synthesized $Ba_{0.85}Sm_{0.1}TiO_3$ has a tetragonal dominant structure with the presence of intermediate $SmTi_2O_3$ at low annealing temperature.
4. The tetragonality, the theoretical density and the crystalline size were increased by increasing annealing temperature.
5. The morphology of the produced sample transferred from nano-cubes to nano-whisker to nano-mace (nano-aggregates) with the increase of annealing temperature.

References

[1] M. Roy, I. Bala, S.K. Barabar, S. Jangid and P. Dave, J. Phys. Chem. Solids, 72 (2011) 1347–1353.
[2] N. Angelescu, Ceramics Int., 24 (1998) 73–76.
[3] H. Schneider, J. Schreuer and B. Hildmann, J. Eur. Ceram. Soc., 28 (2008) 329–344.
[4] Z. Suroviak, M.F. Kupriyanov and D. Czekaj, J. Eur. Ceram. Soc., 21 (2001) 1377.
[5] E. Longo, A.T. de Figueiredo, M.S. Silva, V.M. Longo, V.R. Mastelaro, N.D. Vieira, M. Cilense, R.W.A. Franco and J.A. Varela, J. Phys. Chem. A, 112 (2008) 8953.
[6] Q. Pan, J. Jia, K. Huang and D. He, Mater. Lett., 61 (2007) 1210.
[7] J. König, M. Spreitzer and D. Suvorov, J. Eur. Ceram. Soc., 31 (2011) 1987–1995.
[8] EU Directive 2002/95. http://ec.europa.eu/environment/waste/weee/index_en.htm.

[9] K. Chandramani Singh and A.K. Nath, Mater. Letters, 65 (2011) 970–973.
[10] M.Z.-C. Hu, V. Kurian, E.A. Payzant, C.J. Rawn and R.D. Hunt, Powder Technol., 110 (2000) 2–14.
[11] K.Y. Chen and Y.-W. Chen, Powder Technol., 141 (2004) 69–74.
[12] Y. Mao, S. Mao, Z.-G. Ye, Z. Xie and L. Zheng, Mater. Chem. Phys., 124 (2010) 1232–1238.
[13] T.K. Kundu, A. Jana and P. Barik, Bull. Mater. Sci., 31 (2008) 501–505.
[14] F. Jona and G. Shirane, Ferroelectric crystal, New York (1993).
[15] D. Hennings, A. Schnell and G. Simon, J. Am. Ceram. Soc., 65 (1982) 135.
[16] Y.M. Hu, H.S. Gu, X.C. Sun, J. You and J. Wang, Appl. Phys. Lett., 88 (2006) 193120.
[17] M. Yoshimura and K. Byrappa, J. Mater. Sci., 43 (2008) 2085–2103.
[18] J. Moon, M.L. Carasso, H.G. Krarup, J.A. Kerchner and J.H. Adair, J. Mater. Res., 14 (1999) 866–875.
[19] J. Walker, P. Bryant, V. Kurusingal, C. Sorrell, D. Kuscer, G. Drazic, A. Bencan, V. Nagarajan and T. Rojac, Acta Mater., 83 (2015) 149–159.
[20] A. Udomporn and S. Ananta, Curr. Appl. Phys., 4 (2004) 186.
[21] B. Su, C.B. Ponton and T.W. Button, J. Eur. Ceram. Soc., 21 (2001) 1539.
[22] A. Udomporn, K. Pengpat and S. Ananta, J. Eur. Ceram. Soc., 24 (2004) 185.
[23] M.M. Rashad, R.S. Mohammed, M.M. Hessien, I.A. Ibrahim and A.T. Kandil, J Optoelectron. Adv. Mater., 10 (2008) 1026–1031.
[24] M.M. Hessien, Intern. J. Appl. Nat. Sci., 2 (2013) 9–16.
[25] S. Kim, M.-C. Jun and S.-C. Hwang, J. Am. Ceram. Soc., 82 (1999) 289.
[26] J. Tartaj, J.F. Femandez and M.E.V. Castrejon, Mater. Res. Bull., 36 (2001) 479.
[27] H. Hsien-Lin, G.Z. Cao and I.Y. Shen, Sens. Actuat. A Phys., 214 (2014) 111–119.
[28] A. Rujiwatra, J. Jongphiphan and S. Ananta, Mater. Lett., 59 (2005) 1871.
[29] A. Rujiwatra, N. Thammajak, T. Sarakonsri, R. Wongmaneerung and S. Ananta, J. Cryst. Growth, 289 (2006) 224.
[30] W. Chen and Q. Zhu, Mater. Lett., 61 (2007) 3378–3380.
[31] J. Fang, J. Wang, L.M. Gan and S.C. Ng, Mater. Lett., 52 (2002) 304.
[32] P. Jha, P.R. Arya and A.K. Ganguli, Mater. Chem. Phys., 82 (2003) 355.
[33] E.C. Paris, E.R. Leite, E. Longo and J.A. Varela, Mater. Lett., 37 (1998) 1.
[34] F.M. Pontes, J.H.G. Rangel, E.R. Leite, E. Longo, J.A. Varela, E.B. Araújo and J.A. Eiras, Thin Solid Films., 366 (2000) 232.
[35] S.B. Narang and D. Kaur, Integr. Ferroelectr., 105 (2009) 87.
[36] O.P. Thakura and C. Prakasha, Phase Transit., 76 (2003) 567.
[37] M. Ganguly, S.K. Rout, W.S. Woo, C.W. Ahn and I.W. Kim, Phys. B., 411 (2013) 26–34.
[38] H.W. Lee, S. Moon, C.H. Choi and D.K. Kim, J. Am. Ceram. Soc., 95 (2012) 2429–2434.
[39] A.Q. Jiang, Z.X. Hu and L.D. Zhang, J. Appl. Phys., 85 (1999) 1739–1745.
[40] A. Toyoda, Y. Hamaji, K. Tomono and D.A. Payne, Jpn. J. Appl. Phys., 32 (1993) 4158–4162.
[41] C.H. Perry and B.N. Khanna, Phys. Rev., 105 (1957) 408.
[42] X. Jin, D. Sun, M. Zhang, Y. Zhu and J. Qian, J. Electroceram., 22 (2009) 285.